

Study of the Photobehavior of a Newly Synthesized Chiroptical Molecule: (*E*)-(*R_p*,*R_p*)-1,2-Bis{4-methyl-[2]paracyclo[2](5,8)quinolinophan-2-yl}ethene[†]

Pier Luigi Gentili,^{*,‡} Laura Bussotti,[§] Renzo Ruzziconi,[‡] Sara Spizzichino,[‡] and Paolo Foggi^{‡,§}

Dipartimento di Chimica, Via Elce di Sotto, 8, Università di Perugia (PG), Italy,
LENS, via Nello Carrara 1, Polo Scientifico Universitario, Sesto F.no (FI), Italy

Received: May 11, 2009; Revised Manuscript Received: August 3, 2009

A new chiroptical compound, (*E*)-(*R_p*,*R_p*)-1,2-bis{4-methyl-[2]paracyclo[2](5,8)quinolinophan-2-yl}ethene (*trans*-RPQE) has been synthesized, and its photoresponse has been investigated through steady state and time-resolved absorption and emission spectroscopies and theoretical calculations. To elucidate the relaxation mechanism of *trans*-RPQE after photoexcitation, the photophysics of the 2,4-dimethyl-[2]paracyclo[2](5,8)-quinolinophane chromophore has also been studied. The quantum yields of the different relaxation paths for *trans*-RPQE have been determined. It emerges that in addition to thermal and radiative routes, *trans*-RPQE also photoisomerizes with a quantum yield of 8%. *Trans*- and *cis*-RPQE isomers are pseudoenantiomers exhibiting appreciably different CD spectra, whereby RPQE can be a model for the design of new promising chiroptical photoswitches.

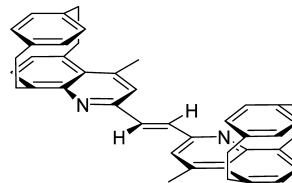
1. Introduction

Photoisomerization around a C=C double bond in olefinic molecules is conceived as one of the most fundamental reactions in photochemistry, and it has long been studied.¹ Recently, renewed interest has been spurred by the development of nanotechnology. In fact, every photoreactive olefin constitutes a molecular machine and a molecular processor; photoinduced *cis*–*trans* isomerization is one of the simplest means of converting light into mechanical motion on the angstrom scale, and it is a way of processing and storing binary information.^{2,3} Chiral photoresponsive alkenes have been attracting pronounced interest since they are asymmetric molecular motors that can influence organization at the supramolecular level, as has been demonstrated for azobenzene derivatives.^{4,5} As chiroptical switches, a nondestructive readout is feasible by monitoring the optical rotation at wavelengths remote from the wavelengths used for switching.⁶ Chiral switching systems based on the C=C photoisomerization can exist both as enantiomeric photobistable molecules, such as axially chiral aryl-methylene cycloalkanes⁷ and helically shaped inherently dissymmetric overcrowded alkenes,⁸ and as pseudoenantiomers; that is, diastereoisomers that show close resemblance and exhibit opposite mirror-image chiral properties, such as some sterically overcrowded alkenes, consisting of an asymmetrical upper part connected via a double bond to a symmetric lower part⁹ or some stilbenophanes.¹⁰

In this work, we present the photobehavior of a newly synthesized chiral 1,2-disubstituted ethylene, (*E*)-(*R_p*,*R_p*)-1,2-bis{4-methyl-[2]paracyclo[2](5,8)quinolinophan-2-yl}ethene, hereinafter indicated as *trans*-RPQE (Scheme 1).

In this compound, the C=C double bond bridges two equivalent 2,4-dimethyl-[2]paracyclo[2](5,8)quinolinophanes. Substituted cyclophanes are drawing much attention because of their planar chirality, which is known to behave quite differently from conventional point chirality in asymmetric

SCHEME 1: Structure of *trans*-RPQE



reactions, catalysis and host–guest interactions.¹¹ In *trans*-RPQE, the two quinolinophane moieties confer planar chirality to the overall molecule, and the *trans* and *cis* isomers, under which the compound can exist, are switchable pseudoenantiomers. Below, we present experimental and theoretical data shedding light on the photophysical and photochemical properties of *trans*-RPQE. Some data regarding the photophysics of 2,4-dimethyl-[2]paracyclo[2](5,8)quinolinophane chromophore (named as RPQ) are reported to elucidate the photobehavior of *trans*-RPQE.

2. Experimental Section

If not specified otherwise, ¹H NMR and ¹³C NMR spectra were recorded at 400 and 100 MHz, respectively, in CDCl₃ solution using tetramethylsilane as an internal standard. IR spectra were recorded in a FT-IR instrument in CHCl₃ solution in the 4000–400 cm⁻¹ range. Optical activity was measured at 20 °C in CHCl₃ solution. UV/vis absorption measurements were performed on a Perkin-Elmer Lambda 800 spectrophotometer. Circular dichroism absorption spectra were recorded on a Jasco J810 instrument.

2.1. Reagents and Solvents. 2,4-Dimethyl[2]paracyclo[2](5,8)quinolinophane (RPQ) and 4-methyl-[2]paracyclo[2](5,8)-quinolinophane-2-carbaldehyde were available from previous works.¹² All the other reagents for the synthesis of *trans*-RPQE were commercial products, and they were used without further purification. Both tetrahydrofuran and diethyl ether were distilled from KOH pellets in the presence of CuCl and redistilled from sodium wire in the presence of the violet-blue benzophenone

[†] Part of the “Vincenzo Aquilanti Festschrift”.

* Corresponding author. Phone: +39 075 5855576. Fax: +39 075 5855598. E-mail: pierluigi.gentili@unipg.it.

[‡] Università di Perugia.

[§] Polo Scientifico Universitario.

sodium ketyl. Acetonitrile ($\geq 99.9\%$, spectrophotometer grade) and chloroform, for the investigation of spectral properties and the photobehavior of RPQE and RPQ, were used as received.

2.2. Synthesis. (*E*)-(R_pR_p)-1,2-Bis[4-methyl-[2]paracyclo[2](5,8)quinolinophan-2-yl]ethene (*trans*-RPQE). Butyllithium (BuLi, 1.70 M in hexanes, 1.41 mL, 2.4 mmol) was added to a solution of (*R*)-2,4-dimethyl[2]paracyclo[2](5,8)quinolinophane (0.62 g, 2.2 mmol) in anhydrous diethyl ether (Et₂O, 20 mL), at 0 °C under nitrogen atmosphere and under stirring. The cold bath was removed, and the mixture was allowed to react 1 h at 20 °C. After cooling at -50 °C, a solution of (*R*)-4-methyl-[2]paracyclo[2](5,8)quinolinophane-2-carbaldehyde (0.65 g, 2.2 mmol) in diethyl ether (3 mL) was added, and the mixture was stirred for 15 min. Then the temperature was allowed to rise to 20 °C, and water (30 mL) was added. The organic phase was separated, the aqueous phase was extracted again with CH₂Cl₂ (3 × 20 mL), and the collected organic phases were dried with Na₂SO₄. After solvent evaporation at reduced pressure, chromatography of the crude product on silica gel (eluent, 8:2 petroleum ether/diethyl ether) allowed recovery of unreacted starting materials (50 mg) and a yellow amorphous solid (1.15 g). The latter was dissolved in acetic acid (120 mL), *p*-toluenesulfonic acid (TsOH, 0.5 g) was added, and the mixture was refluxed for 18 h. After the solvent was evaporated at reduced pressure, 10% aqueous NaOH (20 mL) was added to the residue, and the mixture was extracted with CH₂Cl₂ (3 × 60 mL). The collected organic phases were dried with Na₂SO₄, and the solvent was evaporated at reduced pressure. Chromatography of the crude on silica gel (eluent, 9:1 hexane/diethyl ether) allowed a white amorphous solid to be recovered. Recrystallization from hexane/ethyl acetate mixtures gave 0.68 g (61%) white, flat crystals of a product, which was identified as the expected alkene *trans*-RPQE on the basis of the following spectroscopic and analytical characteristics: mp 168–170 °C (dec). [α]_D²⁰ = -157 (0.32, CHCl₃). ¹H NMR: δ 7.98 (s, 1 H), 7.49 (s, 1 H), 6.93–6.79 (four peaks, AB system, J_{AB} = 7.2 Hz, 2 H), 6.55–6.51 (tight AB system, J_{AB} = 8.2 Hz, 2 H), 5.87 (d, J = 7.6 Hz, 1 H), 5.59 (d, J = 7.6 Hz, 1 H), 4.51 (broad t, J = 10.7 Hz), 3.88 (dd, J = 13.9 and 9.1 Hz, 1 H), 3.28–3.00 (m, 5 H), 2.78 (s, 3 H), 2.69–2.59 (m, 1 H). ¹³C NMR: δ 152.2, 150.5, 143.2, 139.9, 139.8, 137.9, 136.9, 133.9, 133.3, 132.6, 132.5, 131.1, 129.7, 128.6, 128.6, 122.1, 37.7, 35.3, 34.7, 32.1, 22.9. IR (CHCl₃): ν_{\max} 2929, 1587, 1440, 750 cm⁻¹. Anal. Calcd. for C₄₂H₃₈N₂: C, 88.38; H, 6.71; N, 4.91. Found: C, 88.26; H, 6.67; N, 4.78.

2.3. Photophysical and Photochemical Experiments. Corrected emission spectra were recorded using a Spex Fluorolog-21680/1 spectrofluorometer, controlled by Spex DM 3000F spectroscopy software. For fluorescence quantum yield measurements, the absorbances at the excitation wavelengths were kept below 0.1. Anthracene in ethanol (Φ_F = 0.27) was used as standard.¹³

The fluorescence lifetimes were measured with a time-correlated single-photon counting fluorometer (Edinburgh Instruments 199S) using a N₂ lamp as irradiation source.

For time-resolved laser flash photolysis measurements on the nanosecond time scale, the third harmonic (λ_{exc} = 355 nm) of the output from a Continuum Surelite Nd:YAG laser of energy less than 5 mJ per pulse and about 10 ns time resolution was used. Q-switch delays were used to reduce the laser intensity. Spectrophotometric analysis was performed by using a 150 W xenon source, a Baird-Tatlock monochromator blazed at 500 nm, a Hamamatsu R928 photomultiplier, and a Tektronix DSA

602 digital analyzer. The data were processed by a Tektronix PEP 301 computer.

The product $\Phi_T \times \epsilon_T$ for *trans*-RPQE (where Φ_T and ϵ_T are the triplet quantum yield and the molar absorbance coefficient, respectively) was determined by calibrating the experimental setup with optically matched solutions of benzophenone in benzene ($\Phi_T \times \epsilon_T$ = 7200 dm³ mol⁻¹ cm⁻¹ at 520 nm) or in acetonitrile ($\Phi_T \times \epsilon_T$ = 6500 M⁻¹ cm⁻¹ at 520 nm).¹⁴

The triplet quantum yield of *trans*-RPQE in benzene was measured by comparing the changes in absorbance of β -carotene triplet sensitized by energy transfer from the substrate and that sensitized by benzophenone, used as a standard (Φ_T = 1), under the same experimental conditions (absorbance at 355 nm and β -carotene concentration). More details about the method of triplet quantum yield determinations are reported in the literature.¹⁵

The experimental instrumentation and data processing for femtosecond time-resolved transient absorption spectroscopy have been described in detail in previous papers.^{16,17} Tunable excitation pulses are obtained by means of a BBO-based optical parametric generator (OPG) pumped at 1 kHz repetition rate by pulses from an amplified Ti:sapphire laser system (duration ~100 fs at 800 nm, energy 700 μ J/pulse). The wavelength of 372 nm (with average powers of roughly 1 mW) used to excite the *trans*-RPQE was obtained as the fourth harmonic of the OPG signal at 1.5 μ m. A white-light continuum pulse (350–700 nm) was split into two parts of equal intensity by a 50/50 fused-silica–Al beam splitter. One part, acting as a probe beam, was spatially overlapped with the excitation beam inside the sample. The second part crossed the sample in a different position and provided a convenient reference signal. The probe and reference beams were spectrally dispersed in a flat-field 25 cm Czerny–Turner spectrometer and detected by means of a back-illuminated CCD.

Two different configurations of the detection system were utilized to obtain the data sets herein presented, which are composed of both transient spectra (transmittance of the excited state vs wavelength at a given pump–probe delay time) and kinetic plots (intensity of the probe vs delay time at a fixed wavelength).

Recording kinetic plots requires narrow bandwidth detection.¹⁶ The desired wavelengths were selected with 5 nm bandwidth variable interference filter. The intensity of the probe pulse was measured by means of a silicon difference photodiode and a lock-in amplifier synchronized to a chopper, switching the pump pulse on and off at half the repetition rate of the laser system (500 Hz). In this way, the output of the phase-locked amplifier provided the modulation of the probe pulse intensity due to the interaction with the pump pulse. The instrumental function defined as the cross-correlation between the pump and probe pulses measured in the pure solvent by detecting the heterodyned Kerr signal¹⁶ is almost Gaussian, and its time duration is 200 \pm 20 fs (fwhm).

In all the experiments, the relative pump–probe polarization was set to the magic angle (54.7°) to discriminate transient absorption signals against those due to orientational dynamics.

The sample solutions flew through a 1 mm thick calcium fluoride cell connected to a solution reservoir and a pump system. All the samples were dissolved in acetonitrile to obtain an optical density of about 1 at the excitation wavelength. Steady-state absorption spectra of the solutions were measured before and after the experiments to check for possible sample decomposition. All measurements were carried out at room temperature (~22°). Several short exposure time experiments

were carried out to prevent any sample degradation. The presented spectra are obtained as the average of at least five different acquisitions.

For photochemical measurements, a 150 W high-pressure Xe lamp coupled with a monochromator was used. The photoreaction of *trans*-RPQE was monitored by absorption spectrometry through a Perkin-Elmer Lambda 800 spectrophotometer and by HPLC through a Waters 600 chromatograph coupled with an HP 3390A integrator and spectrophotometric detection. The column was a Phenomenex 5u C18 (300A, 250 × 4.60 mm, 5 μm) for analytical purpose, s and a 90/10 acetonitrile/water mixture was used as the eluent. A ferrioxalate actinometer was used for the measurements of photoisomerization quantum yield.

2.4. Calculations. The screening for the most stable conformations of *trans*- and *cis*-RPQE isomers was performed through the semiempirical PM3 method. To determine the nature of the optically active electronic transitions responsible for the bands' appearing in the absorption spectra of *trans*-RPQE and RPQ, semiempirical ZINDO/S¹⁸ calculations were carried out on the geometries optimized by PM3 method for the electronic ground states. The HyperChem program was used for all the calculations.

3. Results and Discussion

3.1. Synthesis. *Trans*-RPQE was prepared with a yield of 61% by condensation of (*R_p*)-2-lithiomethyl-4-methyl-[2]paracyclo[2](5,8)quinolinophane¹² with (*R_p*)-4-methyl-[2]paracyclo[2](5,8)quinolinophane-2-carbaldehyde, followed by acid-catalyzed dehydration of the resulting alcohol (Scheme 2).

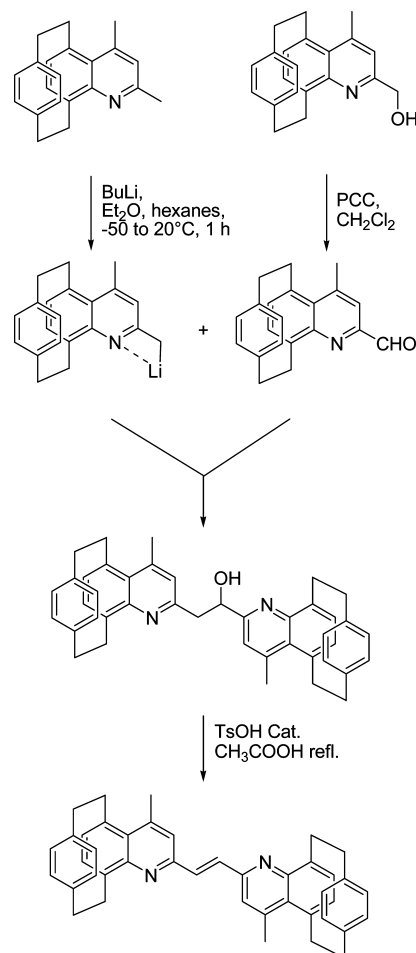
Like in [2.2]paracyclophane (PCP), repulsive interactions make the faced homocyclic ring of [2]paracyclo[2](5,8)quinolinophane moiety bent and boat-shaped. Because of a reduced inter-ring repulsion due to the electron-drawing effect of the adjacent pyridine ring, most probably, the distance between the overlapping benzene ring planes, defined by the four carbon atoms not connected to the bridging methylene carbon atoms, is shorter than the respective distance in PCP (3.099 Å).¹⁹ For the same reason, the out-of-plane deformation of the two-faced aromatic rings should be lower than in PCP (12.6°) and should also be different for the two rings.

Trans-RPQE can exist as a large ensemble of conformational isomers by virtue of the free rotation of the [2]paracyclo[2](5,8)quinolinophane moieties around their quasi-single C–C bonds.²⁰ However, the three most stable rotamers are *s-trans*, *s-trans* (**A_t**), *s-trans*, *s-cis* (**B_t**) and *s-cis*, *s-cis* (**C_t**), (see Figure 1). Their structures have been optimized by the PM3 method. From their energies and statistical weights calculated at 298 K (reported in Table 1), it results that **A_t** is the most stable and abundant rotamer for *trans*-RPQE.

The ¹H NMR spectrum of *trans*-RPQE confirms the theoretical prediction. In fact, the ethylenic protons (H^E) give rise to a singlet at δ 7.98 ppm. This excludes conformer **B_t**, since its structure entails two chemically unequal ethylenic protons that should exhibit distinct signals. According to PM3 calculations, the H^E–H³ distance should be 2.24 Å in conformation **A_t** and 2.40 Å in conformation **C_t**. Since proton H^E at δ 7.98 exhibits a low-intensity NOE contact with the H³ proton at δ 7.49, a distance of 2.23 Å between H^E–H³ has been calculated,²¹ which provides additional evidence in favor of **A_t** conformation as the main, if not exclusive, conformation of (*E*)-(*R_p*,*R_p*)-1,2-bis{4-methyl-[2]paracyclo[2](5,8)quinolinophan-2-yl}ethene.

3.2. Steady-State Absorption and Luminescence Properties. *Trans*-RPQE consists of two kinds of chromophores: an ethylene group bridging two equivalent 4-methyl-[2]paracyclo-

SCHEME 2: Synthesis of *trans*-RPQE^a



^a PCC is pyridinium dichromate. For the meaning of the other symbols, see the Experimental section.

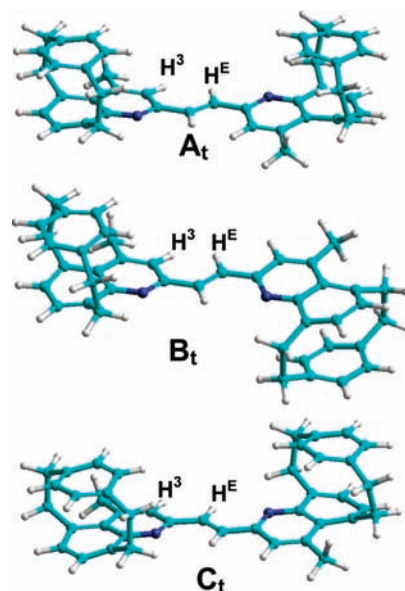


Figure 1. The three most stable conformers of *trans*-RPQE: *s-trans*, *s-trans* (**A_t**), *s-trans*, *s-cis* (**B_t**), and *s-cis*, *s-cis* (**C_t**).

[2](5,8)quinolinophanes. In these chromophores, the facing benzene rings are puckered, since the carbon atoms of the rings bearing the methylene bridges are bent out of the plane of the other sets of four carbon atoms. The planes defined by the two sets of four carbon atoms are separated by a distance shorter

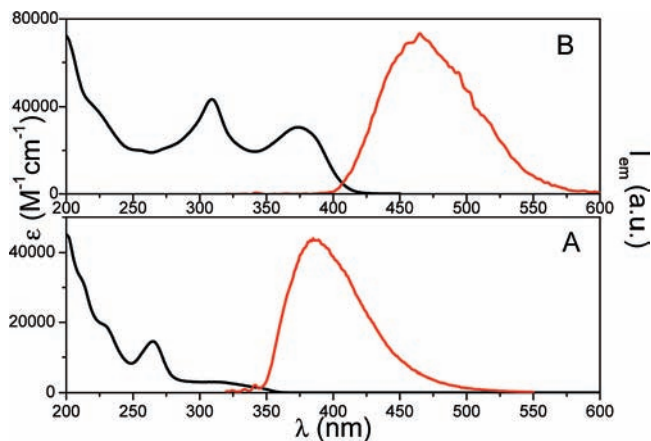
TABLE 1: Energies and Boltzmann Population (calculated at 298 K) for the Three Most Stable Rotamers of *trans*-RPQE

rotamer	energy (KJ/mol)	% population $T = 298$ K
A_t (s-trans, s-trans)	-567 083.10	53.27
B_t (s-trans, s-cis)	-567 080.70	20.24
C_t (s-trans, s-cis)	-567 081.36	26.49

than 3.099 Å; that is, less than the sum of the van der Waals radii (~3.4 Å), whereby their π orbitals interact through space. The absorption spectrum of 2,4-dimethyl-[2]paracyclo[2]-(5,8)quinolinophanes (RPQ) is depicted in Figure 2A along with its emission spectrum. RPQ shows allowed electronic transitions at 210, 228, and 265 nm and a partially allowed transition at 312 nm. According to the ZINDO/S calculations, the absorption at the lowest energy is a HOMO–LUMO “through space” transition having charge transfer character from benzene to the quinoline moiety (see Table 2 for the shape of orbitals). The electronic transitions at higher energies are combinations of pure π , π^* transitions in the donor or acceptor part of the molecule. The emission spectrum of RPQ has a maximum at 386 nm, and it exhibits a large Stokes shift: $\Delta\bar{\nu} = 6077$ cm⁻¹. Its fluorescence quantum yield (Φ_F for $\lambda_{exc} = 310$) and lifetime (τ_F) are 0.047 and 2.0 ns, respectively, in the presence of O₂, and $\Phi_F = 0.058$ and $\tau_F = 2.4$ ns in deoxygenated solution.

In *trans*-RPQE, the π orbital of the ethylene group assures electronic conjugation between the two paracycloquinolinophanes, whereby *trans*-RPQE absorption spectrum is bathochromically shifted with respect to that of RPQ (see Figure 2B). The absorption spectrum of *trans*-RPQE consists of three main allowed transitions at 220, 309, and 375 nm. ZINDO/S calculations reveal that the HOMO–LUMO transition has a “through-space” charge transfer (CT) character from the benzene rings of the two RPQ groups to the two quinolines conjugated with the ethylene, as can also be inferred by observing the representation of orbitals in Table 2. The bands appearing at higher energies are mainly due to “through-bond” π , π^* transitions involving the ethylene and the two RPQ groups beside a less relevant contributions from the CT transition.

Trans-RPQE emission occurs in the visible region: the fluorescence spectrum is centered at 464 nm with a Stokes shift of 5115 cm⁻¹. *Trans*-RPQE fluoresces more strongly than RPQ, since its fluorescence quantum yield is 0.13 in the presence of O₂ and 0.14 in deoxygenated conditions. Moreover, its fluorescence lifetime is longer than that of RPQ, since it lasts 3.7 ns in the presence of oxygen and 4.2 ns without O₂.

**Figure 2.** Absorption (black) and fluorescence (red) spectra of RPQ (A) and *trans*-RPQE (B) in acetonitrile.

3.3. Photochemistry. *Trans*-RPQE presents a stilbenoid structure; therefore, it is expected to photoisomerize upon irradiation, as stilbenes do. When a solution of *trans*-RPQE in acetonitrile is subject to UV irradiation ($\lambda_{irr} = 372$ nm), a spectral evolution is observed, such as that depicted in Figure 3A. The absorbance of the bands centered at 374 and 309 nm wanes; on the other hand, in the spectral region below 290 nm, absorbance slightly increases, whereas at 290 nm, it does not change at all; that is, at 290 nm, there is an isosbestic point.

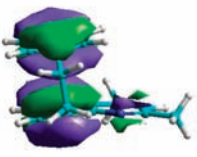
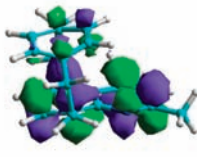


To gather additional information on the photoreaction, chromatographic analyses were carried out. They revealed that the observed spectral evolution of Figure 3A is due to a neat photoreaction of *trans* isomer, without byproduct formation. The absorption spectrum of the product, separated chromatographically, is shown in Figure 3B, along with that of the *trans* isomer, as a matter of comparison. The product is thermally stable and can be converted back to the reagent upon irradiation. From its photoswitching and its spectral properties, it can be inferred that the photoproduct is the *cis*-RPQE isomer: as expected, the *trans*-to-*cis* conversion is photoreversible and entails a hypsochromic shift and a reduction of allowance for the electronic transitions at lower energies because in the *Z* isomer, the structural steric hindrance reduces the coplanarity of the molecular chromophores. The quantum yield of photoisomerization (Φ_{PC}) has been determined (see the Experimental section for the details) to be 0.082. The photostationary state, achievable by irradiating at 372 nm, consists of a molar fraction of *cis*-RPQE equal to 0.48.

Cis-RPQE can exist under three main conformers: s-*trans*, s-*trans* (**A_c**), s-*trans*, s-*cis* (**B_c**), and s-*cis*, s-*cis* (**C_c**), whose structures, optimized by PM3 method, are depicted in Figure 4.

According to the PM3 calculations, **B_c** is the most stable conformer: it has the most planar structure and less distorted ethylene group. This species is the predominant, if not exclusive, rotamer for *cis*-RPQE (in Table 3, the energies and statistical weights of the conformers, calculated in vacuum at 298 K, are reported).

The *trans*-to-*cis* photoisomerization entails noticeable variations in the CD spectrum (see Figure 5). The *trans* isomer exhibits a broad negative Cotton effect between 420 and 305 nm, followed by a strong and broad positive Cotton effect between 305 and 246 nm. Below 246 nm, two opposite CD bands are present: one negative centered at 227 nm ($\Delta\epsilon = -1194$ M⁻¹ cm⁻¹) and one positive at 203.5 nm ($\Delta\epsilon = +790$ M⁻¹ cm⁻¹). On the other hand, in the CD spectrum of the *cis* isomer, apart from a slight negative Cotton effect between 420 and 386 nm, strong and broad positive Cotton effects are included between 386 and 280.5 nm, consisting of two bands centered at 360 and 289 nm. At wavelengths shorter than 289 nm, a sequence of negative/positive CD bands is present ($\Delta\epsilon = -702$ M⁻¹ cm⁻¹ at 268 nm, $\Delta\epsilon = +70$ M⁻¹ cm⁻¹ at 252 nm, $\Delta\epsilon = -146$ M⁻¹ cm⁻¹ at 242 nm, $\Delta\epsilon = +1326$ M⁻¹ cm⁻¹ at 225 nm, and $\Delta\epsilon = -1034$ M⁻¹ cm⁻¹ at 203 nm). Comparing the CD spectra, it is evident that the two pseudoenantiomers, *trans*- and *cis*-RPQE, show some opposite Cotton effects, especially in the spectral region located at higher energies wherein electronic transitions mainly localized in the [2]paracyclo-[2](5,8)quinolinophane chromophores contribute. According to the DeVoe model,²² the seminal paper of Mason,²³ and the case of two chiral biquinolinophanes²⁴ previously studied, the spectral differences shown in Figure 5 are mainly attributable to the different spatial orientation of the two chiroptical [2]paracyclo[2](5,8)quinolinophane chromophores. In fact, in the

TABLE 2: HOMO and LUMO Orbitals for RPQ and *trans*-RPQE

Compound	HOMO	LUMO
RPQ		
<i>trans</i> -RPQE A_t conformer		

most stable conformer of *trans*-RPQE, A_t , having *s*-*trans*, *s*-*trans* geometry, the two [2]paracyclo[2](5,8)quinolinophanes are oppositely oriented, and they form dihedral angles of 5.3° and 6.5° (according to the PM3 calculations) with respect to the plane defined by the C=C bond, whereas in the most stable conformation of *cis*-RPQE, B_c , having *s*-*trans*, *s*-*cis* geometry, the two chiroptical chromophores have a different mutual orientation and form dihedral angles of 22.1° and 25.4° with respect to the plane defined by the double C=C bond.

3.4. Time-Resolved Absorption Spectra. The picture of the overall relaxation dynamics of *trans*-RPQE after photoexcitation has been completed by means of transient absorption spectroscopies. The spectral evolution included in the time scale from tens of nanoseconds to milliseconds has been recorded by the nanosecond flash photolysis technique, and it is reported in Figure 6. Soon after laser excitation ($\lambda_{exc} = 355$ nm), a positive broadband extending over the entire visible region and with a maximum at 510 nm, along with two negative bands peaked at 370 and 310 nm, was observed. All these bands decayed with the same time constant of 3.3×10^5 s $^{-1}$ (determined in the absence of oxygen), suggesting the involvement of just one transient species.

The bands at 370 and 310 nm, with negative values of ΔOD , are due to the bleaching of the ground state of *trans*-RPQE, whereas the band centered at 510 nm, with positive values of ΔOD , can be attributed to the triplet state of *trans*-RPQE, since its lifetime is shortened through diffusional quenching by oxygen ($k_q = 2.5 \times 10^9$ s $^{-1}$ M $^{-1}$), and it sensitizes the triplet state of

β -carotene. Sensitization experiments, carried out with the purpose of determining the triplet quantum yield of *trans*-RPQE, were unsuccessful when benzophenone ($E_T = 287$ kJ/mol) 14 and biacetyl ($E_T = 236$ kJ/mol) were used as triplet energy acceptors, whereas they were successful with β -carotene ($E_T = 88$ kJ/mol). Therefore, it can be inferred that the triplet energy of *trans*-RPQE is smaller than 236 kJ/mol but larger than 88 kJ/mol. By means of the procedure mentioned in the experimental section, the following values were obtained in benzene at 520

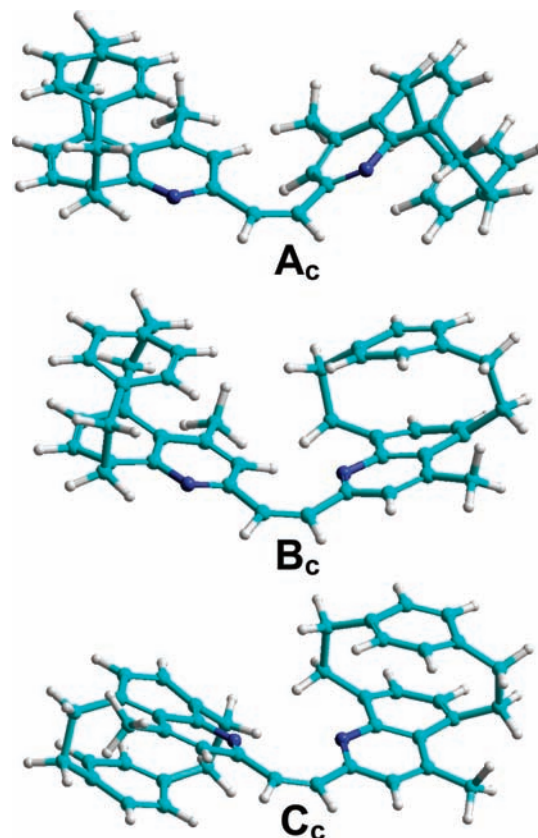


Figure 4. The three most stable rotamers for *cis*-RPQE: *s*-*trans*, *s*-*trans* (A_c), *s*-*trans*, *s*-*cis* (B_c), and *s*-*cis*, *s*-*cis* (C_c).

TABLE 3: Energies and Boltzmann Population (calculated at 298 K) for the Three Rotamers of *cis*-RPQE

rotamer	energy (KJ/mol)	% population $T = 298$ K
A_c (<i>s</i> - <i>trans</i> , <i>s</i> - <i>trans</i>)	-567 039.22	0.08
B_c (<i>s</i> - <i>trans</i> , <i>s</i> - <i>cis</i>)	-567 056.73	99.91
C_c (<i>s</i> - <i>trans</i> , <i>s</i> - <i>cis</i>)	-567 031.56	0.01

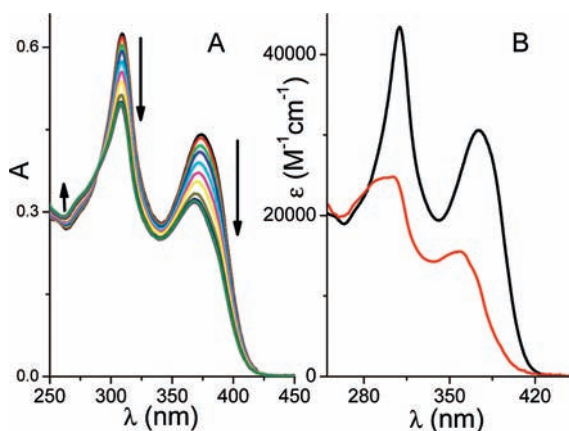


Figure 3. (A) Spectral evolution (highlighted by the arrows) for *trans*-RPQE solved in CH_3CN and irradiated at 372 nm by a Xe lamp for 2 h and 20 min. (B) Absorption spectra for *trans*-RPQE (in black) and *cis*-RPQE (in red) in CH_3CN .

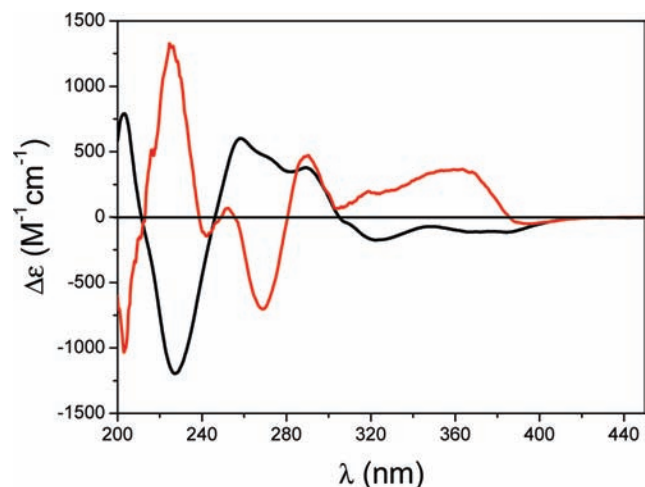


Figure 5. CD spectra for *trans*-RPQE (in black, $C = 3.2 \times 10^{-4}$ M) and *cis*-RPQE (in red, $C = 3.0 \times 10^{-4}$ M) in CH_3CN .

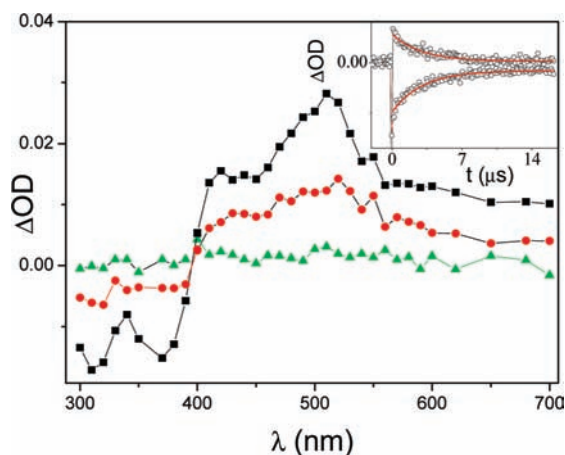


Figure 6. Transient absorption spectra for *trans*-RPQE ($C = 2.5 \times 10^{-5}$ M) in acetonitrile at different delay times after the laser shot ($\lambda_{\text{exc}} = 355$ nm): after 80 ns (black square); after 1.04 μs (red circle) and after 15 μs (green triangle). Inset: kinetics at 570 and 360 nm, fitted by monoexponential functions.

nm: $\Phi_{\text{T}} \times \varepsilon_{\text{T}} = 3600 \text{ M}^{-1} \text{ cm}^{-1}$ (where Φ_{T} is the triplet quantum yield and ε_{T} is the triplet absorption coefficient), $\Phi_{\text{T}} = 0.42$ and $\varepsilon_{\text{T}} = 8570 \text{ M}^{-1} \text{ cm}^{-1}$. It follows that the rate constant for the intersystem crossing $S_1 \rightarrow T_1$ is $k_{\text{ISC}}^{\text{I}} = (\Phi_{\text{T}}/\tau_{\text{F}}) = 1 \times 10^8 \text{ s}^{-1}$.

To take snapshots of the molecular states preceding the population of the triplet state of *trans*-RPQE, pump–probe experiments with femtosecond resolution were performed. The spectral evolution recorded for *trans*-RPQE (in CH_3CN , $\lambda_{\text{irr}} = 372$ nm) is reported in Figure 7.

The excitation at 372 nm activates the “through space” CT transition described in Section 3.2 entailing an instantaneous appearance of two bands in the visible region: one is centered at 424 nm, whereas the other, broader is peaked at 650 nm and presents a shoulder centered at 550 nm. The rises of these features are well-described by the convolution of a step function (instantaneous response) with the instrumental function as it is shown in Figure 8A and D. Then the intensity of the red portion of the spectrum undergoes a slight decrease. This spectral decay is well-fitted by a monoexponential function with a decay time of 70 ps detectable at both 510 and 625 nm (see Figure 8B and E, respectively). Finally, the shape of the spectrum also evolves (Figure 7), and it becomes resemblant with the spectrum of the triplet state of *trans*-RPQE. This is evident by comparing the

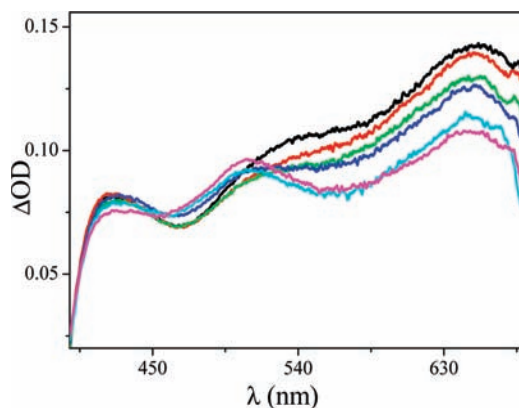


Figure 7. Transient absorption spectra for *trans*-RPQE pumped at 372 nm in acetonitrile ($C = 2.5 \times 10^{-5}$ M), for delay times of 1 ps (black line), 10 ps (red line), 200 ps (green line), 500 ps (blue line), 1 ns (cyan line), 1.5 ns (magenta line).

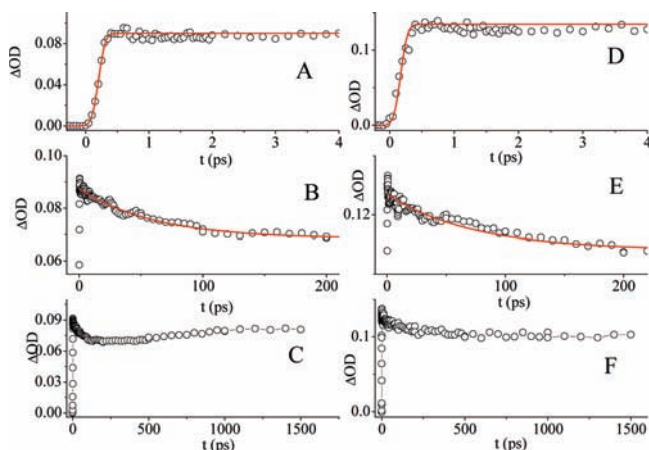
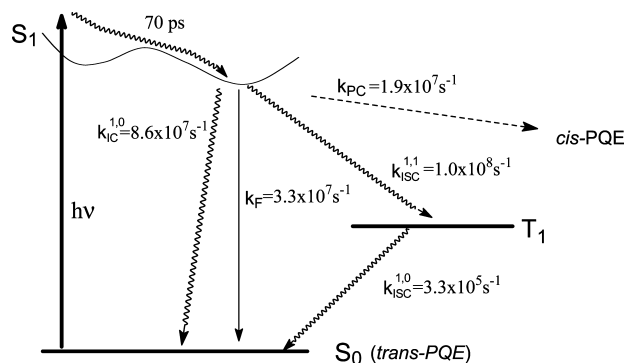


Figure 8. Kinetic traces recorded at 510 nm (A, B, and C) and 625 nm (D, E, and F) for *trans*-RPQE pumped at 372 nm in acetonitrile ($C = 2.5 \times 10^{-5}$ M). The first portions of the kinetics (A and D) are fitted by a convolution of a step function with the instrumental function (red traces). The following decays, evidenced by zooming in along the y-axis (B and E), are well-fitted by monoexponential functions (red traces).

last spectrum of Figure 7 (yellow trace) with the first transient spectrum of Figure 6 (black square): both show a peak centered at 510 nm, presenting two shoulders at shorter and longer wavelengths. This spectral evolution determines a slight increase in ΔOD values at 510 nm and a slight decrease in ΔOD at 625 nm (see Figure 8C and F, respectively).

The nature of the spectral evolution observed in Figure 7 and its time amplitude suggest that as soon as the “through space” CT state is populated by absorption of the pump, a restricted structural rearrangement accompanied by vibrational relaxation (as it occurs in stilbene and some of its derivatives)^{25–29} follows, leading most likely to a potential energy well in the S_1 state, from where *trans*-RPQE can evolve to its triplet state; to its ground state; and to the product, *cis*-RPQE. The time window detectable by our femtosecond apparatus does not allow the complete decay of the S_1 state to be followed, since it occurs in 4.2 ns. Just the first steps of the S_1 state decay can be correctly evaluated since the long decay time provides an almost flat trace in the 1.5 ns window.

3.5. Concluding Remarks. This work provides insight into the relaxation dynamics following photoexcitation of the newly synthesized chiroptical *trans*-RPQE. Although the molecule can exist as three main rotamers, theoretical and experimental evidence suggest that the s-*trans*, s-*trans* (A_t) is the most

SCHEME 3: Schematic Representation of the Relaxation Mechanism after Photoexcitation for *trans*-RPQE

TABLE 4: Survey of the Quantum Yields and Kinetic Constants for the Different Relaxation Paths Concerning *trans*-RPQE

quantum yields	kinetic constants (s ⁻¹)
$\Phi_F = 0.14$	$k_F = 3.3 \times 10^7$
$\Phi_T = 0.42$	$k_T = 1.0 \times 10^8$
$\Phi_{PC} = 0.082$	$k_{PC} = 1.9 \times 10^7$
$\Phi_{IC} = 0.36$	$k_{IC} = 8.6 \times 10^7$

abundant conformer in acetonitrile at room temperature. The excitation of *trans*-RPQE into the lowest energy band triggers a “through space” CT transition. The Franck–Condon state, giving rise to absorptions extended over the entire visible region, relaxes in 70 ps to a minimum well of the S_1 state, as depicted in Scheme 3.

From this minimum in S_1 , several relaxation routes are available: radiative and thermal decay to S_0 , intersystem crossing to T_1 , and isomerization to the *s-trans*, *s-cis* rotamer of *cis*-RPQE. The different paths of relaxation are undertaken with rates conferring to the S_1 state a lifetime of 4.2 ns. A survey of quantum yields and kinetic constants for the different decay routes are reported in Table 4.

The most likely processes to occur are the thermal relaxations to the T_1 and S_0 states, but the colored fluorescence of *trans*-RPQE is also not negligible nor the *trans*-to-*cis* isomerization. Although the photoreaction takes place with a low quantum yield, it entails significant changes in the CD spectrum that could be exploited in the molecular computing field.

Acknowledgment. Fundings from the Italian FIRB 2004 “Molecular compounds and hybrid nanostructured materials with resonant and nonresonant optical properties for photonic devices” (Contract no. RBNE033KMA), from the European Community under the contract RIII-CT-2003-506350, and from the Ente Cassa di Risparmio di Firenze are acknowledged. The authors thank Mr. D. Pannacci of the Department of Chemistry (University of Perugia) for his support in chromatographic determination of the reaction quantum yield and L. Gonnelli of CERM (University of Florence) for his support in CD measurements.

References and Notes

- (1) Saltiel, J.; Charlton, J. L. *Cis-Trans Isomerization of Olefins in Rearrangements in Ground and Excited States*; de Mayo, P., Ed.; Academic Press: New York, 1980; Vol. 3.
- (2) (a) *Molecular Machines and Motors*; Sauvage, J.-P., Ed.; Springer-Verlag: Berlin, London, 2001; Vol. 99. (b) Drexler, K. E. *Nanosystems: Molecular Machinery, Manufacturing and Computation*; John Wiley & Sons: New York, 1992.
- (3) Pollard, M. M.; ter Wiel, M. K. J.; van Delden, R. A.; Vicario, J.; Koumura, N.; van den Brom, C. R.; Meetsma, A.; Feringa, B. L. *Chem.—Eur. J.* **2008**, *14*, 11610–11622.
- (4) Alam, M. Z.; Yoshioka, T.; Ogata, T.; Nonaka, T.; Kurihara, S. *Chem.—Eur. J.* **2007**, *13*, 2641–2647.
- (5) van Delden, R. A.; Mecca, T.; Rosini, C.; Feringa, B. L. *Chem.—Eur. J.* **2004**, *10*, 61–70.
- (6) Feringa, B. L.; van Delden, R. A.; Koumura, N.; Geertsema, E. M. *Chem. Rev.* **2000**, *100*, 1789–1816.
- (7) Lemieux, R. P.; Schuster, G. B. *J. Org. Chem.* **1993**, *58*, 100–110.
- (8) Huck, N. P. M.; Jager, W. F.; de Lange, B.; Feringa, B. L. *Science* **1996**, *273*, 1686–1688.
- (9) van Delden, R. A.; Hurenkamp, J. H.; Feringa, B. L. *Chem.—Eur. J.* **2003**, *9*, 2845–2853.
- (10) Rajakumar, P.; Selvam, S. *Tetrahedron* **2007**, *63*, 8891–8901.
- (11) *Modern Cyclophane Chemistry*; Gleiter, R., Hopf, H., Eds.; Wiley-VCH: Weinheim, Germany, 2004. (b) Gibson, S. E.; Knight, J. D. *Org. Biomol. Chem.* **2003**, *1*, 1256–1269. (c) Vögtle, F. *Cyclophane Chemistry*; Wiley: New York, 1993.
- (12) (a) Ruzziconi, R.; Piematti, O.; Ricci, G.; Vinci, D. *Synlett* **2002**, *5*, 747–750. (b) Ruzziconi, R.; Ricci, G. *Tetrahedron-Asymmetry* **2005**, *16*, 1817–1827.
- (13) Melhuish, W. H. *J. Phys. Chem.* **1961**, *65*, 229–235.
- (14) Murov, S. L.; Carmichael, I.; Hug, G. L. In *Handbook of Photochemistry*; Marcel Dekker Inc.: New York, 1993.
- (15) Kumar, C. V.; Qin, L.; Das, P. K. *J. Chem. Soc. Faraday Trans. 2* **1984**, *80*, 783–793.
- (16) (a) Neuwahl, F. V. R.; Bussotti, L.; Foggi, P. *Res. Adv. Photochem. Photobiol.* **2000**, *1*, 77–94. (b) Salvi, P. R.; Moroni, L.; Neuwahl, F. V. R.; Foggi, P. *J. Phys. Chem. A* **2003**, *107*, 1689–1696. (c) Ameer-Beg, S.; Ormson, S. M.; Poteau, X.; Brown, R. G.; Foggi, P.; Bussotti, L.; Neuwahl, F. V. R. *J. Phys. Chem. A* **2004**, *108*, 6938–6943. (d) Gentili, P. L.; Bussotti, L.; Righini, R.; Beni, A.; Bogani, L.; Dei, A. *Chem. Phys.* **2005**, *314*, 9–17. (e) Marcelli, A.; Foggi, P.; Moroni, L.; Gellini, C.; Salvi, P. R. *J. Phys. Chem. A* **2008**, *112*, 1864–1872. (f) Moroni, L.; Gellini, C.; Salvi, P. R.; Marcelli, A.; Foggi, P. *J. Phys. Chem. A* **2008**, *112*, 11044–11051.
- (17) (a) Lewis, J. D.; Bussotti, L.; Foggi, P.; Perutz, R. N.; Moore, J. J. *Phys. Chem. A* **2002**, *106*, 12202–12208. (b) Gentili, P. L.; Mugnai, M.; Bussotti, L.; Righini, R.; Foggi, P.; Cicchi, S.; Ghini, G.; Viviani, S.; Brandi, A. *J. Photochem. Photobiol., A* **2007**, *187*, 209–221.
- (18) Bacon, A. D.; Zerner, M. C. *Theor. Chim. Acta* **1979**, *53*, 21–54.
- (19) Starikova, Z. A.; Fedyanin, I. V.; Antipin, M. Yu. *Russ. Chem. Bull., Int. Ed.* **2004**, *53*, 1779–1805.
- (20) Mazzucato, U.; Momicchioli, F. *Chem. Rev.* **1991**, *91*, 1679–1719.
- (21) H^E-H^F average distance has been calculated by the equation: $r_{H^E-H^F} = r_{H^E-CH_3} \times (\eta_{H^E}/\eta_{CH_3})^{1/6}$ considering the H^3-4-CH_3 average distance of 3.02 Å as the internal standard and assuming the initial rate approximation being valid for all interactions.
- (22) Superchi, S.; Giorgio, E.; Rosini, C. *Chirality* **2004**, *16*, 422–451.
- (23) Mason, S. F.; Seal, R. H.; Roberts, D. R. *Tetrahedron* **1974**, *30*, 1671–1682.
- (24) Ricci, G.; Ruzziconi, R.; Giorgio, E. *J. Org. Chem.* **2005**, *70*, 1011–1018.
- (25) Greene, B. I.; Hochstrasser, R. M.; Weisman, R. B. *Chem. Phys. Lett.* **1979**, *62*, 427–430.
- (26) Iwata, K.; Hamaguchi, H. *J. Phys. Chem. A* **1997**, *101*, 632–637.
- (27) Park, N. S.; Waldeck, D. H. *Chem. Phys. Lett.* **1990**, *168*, 379–384.
- (28) Lee, M.; Haseltine, J. N.; Smith, A. B., III; Hochstrasser, R. M. *J. Am. Chem. Soc.* **1989**, *111*, 5044–5051.
- (29) Tan, X.; Gustafson, T. L.; Lefumeux, C.; Burdzinski, G.; Buntinx, G.; Poizat, O. *J. Phys. Chem. A* **2002**, *106*, 3593–3598.